Distribution Agreement

In presenting this thesis as a partial fulfillment of the requirements for a degree from Emory University, I hereby grant to Emory University and its agents the non-exclusive license to archive, make accessible, and display my thesis in whole or in part in all forms of media, now or hereafter now, including display on the World Wide Web. I understand that I may select some access restrictions as part of the online submission of this thesis. I retain all ownership rights to the copyright of the thesis. I also retain the right to use in future works (such as articles or books) all or part of this thesis.

Andrew Vu April 17, 2013

Visualizing Spacetime Curvature in Black Hole Mergers using Tendex and Vortex Lines

by

Andrew Vu

Dr. Fereydoon Family

Department of Physics

Adviser

Dr. Pablo Laguna

Center for Relativistic Astrophysics

Georgia Institute of Technology

Adviser

Dr. Richard Williamon

Committee Member

Dr. David Borthwick

Committee Member

2013

Visualizing Spacetime Curvature in Black Hole Mergers using Tendex and Vortex Lines

by

Andrew Vu

Dr. Fereydoon Family

Adviser

Dr. Pablo Laguna

Adviser

An abstract of

a thesis submitted to the Faculty of Emory College of Arts and Sciences

of Emory University in partial fulfillment

of the requirements of the degree of

Bachelor of Sciences with Honors

Department of Physics

2013

Abstract

Visualizing Spacetime Curvature in Black Hole Mergers using Tendex and Vortex Lines

By Andrew Vu

The Weyl curvature tensor (traceless component of the Riemann curvature tensor), which details all the information about the curvature of the local geometry, can be covariantly split into two parts, which are spatial, symmetric, and trace-free. The two tensors are the "electric" part which is the tidal field $\mathcal{E}_{ij}$, which details the stretching and compressing of an observer, and the "magnetic" part which is the frame-drag field $\mathcal{B}_{ij}$, which details the precession of an observer. Each $\mathcal{E}_{ij}$ and $\mathcal{B}_{ij}$ tensor has three orthogonal eigenvector fields that can be visualized by their integral curves. The integral curves of the $\mathcal{E}_{ij}$ field are called the tendex lines, and for the $\mathcal{B}_{ij}$ field are the vortex lines. It follows that each eigenvector's eigenvalue is its tendicity or vorticity, respectively. These lines prove to be a useful tool, as we will show in this paper, for understanding the nonlinear dynamics around regions of strong-gravity such as a stationary black hole, a rotating black hole, and binary black hole merger.

Visualizing Spacetime Curvature in Black Hole Mergers using Tendex and Vortex Lines

by

Andrew Vu

Dr. Fereydoon Family

Adviser

Dr. Pablo Laguna

Adviser

An abstract

a thesis submitted to the Faculty of Emory College of Arts and Sciences

of Emory University in partial fulfillment

of the requirements of the degree of

Bachelor of Sciences with Honors

Department of Physics

2013

Acknowledgements

I would like to acknowledge my sincerest gratitude to Dr. Fereydoon Family for facilitating my learning experience throughout my time at Emory University. Dr. Family has been with me through every ordeal and joy since the first day I met him in my second year, and I have learned so much from being in his Modern Physics and Computational Physics classes and from being his mentee. I would also like to thank Dr. Vincent Boi Hanh Huynh for his personal and academic advice and support throughout my undergraduate years. I would like to thank Dr. Richard Williamon for giving me the encouragement and fuel for my passion in astrophysics. I would like to thank Dr. Pablo Laguna and his Numerical Relativity group, Tanja Bode and Matt Kinsey, at Georgia Tech for their help on the theory and implementation of this project.

Contents

List of Figures

1 Introduction

I was fortunate enough to study general relativity and Maxwell's theory in the same semester last spring. Why was I fortunate you might ask? Well, as I was gradually indulging myself with the words of Carroll and Griffiths, I was comparing these two theories and realized that they are not that far from being different from one another. Albert Einstein came up with special relativity to fit Maxwell's equations back into the Newtonian principles. Formulating his theory of general relativity soon after special relativity, there is bound to be some similarities between general relativity and Maxwell's theory. For one, I noticed that the Coulomb force for an electrostatic charge is very similar to the gravitational force between two objects in equilibrium. And we can draw concentric circles representing the gravitational field outside the Earth in the same way as we do for an electric field outside a charged sphere. Continuously pondering made me ask, does there then exist a Lorentz force equivalent for gravity? Then if so, what is the gravitational analog of the magnetic field? And does there exist the gravitation version of Maxwell's equations?

With the growth of supercomputing clusters and advanced instrumentation, we have seen a tremendous advancement in the study of Einstein's theory of general relativity. In particular, the two-body problem in general relativity has finally been solved, and we now are exploring black hole mergers and observing some peculiar phenomena such as spin-flip, black hole recoil, and orbital hang-up [1][2]. With the construction of LIGO and eLISA for gravitational wave detection, there now leaves an extensive task for data analysis. As of now, the best method for finding a gravitational wave is to match it against a library of waveform templates. These templates are created using numerical relativity which solves the Einstein field equations using complex

algorithms on large supercomputer clusters [3]. By matching the gravitational waves with a library of waveforms, we can then be able to identify the physical phenomena that generated the gravitational radiation. As of now, the most promising source for gravitational wave detection is the radiation given off by the collisions and mergers of binary black holes [4]. Currently, we are in need of new tools that will aid us in the generation of more accurate waveform templates for the analysis of black hole mergers. What I will try to do is implement a code in the numerical simulations to produce lines that are analogous to the electric and magnetic field lines in Maxwell's theory [5]. These lines, called the tendex and vortex lines, represent the tidal forces and frame-dragging effects on an observer in space. By implementing this tool, I hope to understand the nonlinear dynamics of curved spacetime in regions of strong-gravity, like those near the horizon of rotating black holes and black hole mergers [6]. In all, the visualization of these lines will give us insight on new ways to generate the gravitational waveforms emitted by black hole mergers [4].

This paper is organized into four main sections. The first section is a brief introduction to general relativity starting with special relativity and the metric tensor to the Schwarzschild solution and linearized gravity. The second section deals with gravitational waves, the detectors, and major sources of gravitational radiation. The third section introduces the theoretical equations behind the tool that I will be using to visualize curved spacetime dynamics. And for section four, I will discuss my procedure for the implementation of this tool and present my results for single black holes and binary black hole systems.

1.1 Space, Time and Special Relativity

In Newtonian physics, space and time are separate. Time is absolute, and gravity, which is considered instantaneous, is described by [7]

$$\vec{a}_g = -\nabla\Phi; \qquad \text{where } \Phi(\vec{r}) = \int -\frac{G\rho(\vec{r}')}{\|\vec{r}-\vec{r}'\|}d^3\vec{r}' \ . \tag{1.1}$$

In Galilean relativity, the laws of physics are unchanged for observers in different inertial frames, or observers moving at constant velocities [8]. With the addition of Maxwell's equations describing electromagnetism, the speed of light was calculated and determined to be constant by the Michelson-Morley experiment. This discrepancy led Albert Einstein to develop the theory of special relativity in order to explain the inconsistency of Maxwell's equations with Galilean relativity [7]. In special relativity, the speed of light is constant in all inertial frames and Maxwell's equations are satisfied in all inertial frames. In addition, Einstein postulated that moving observers see time and space differently in the direction of motion (time dilation and length contraction) which is described by [9]

$$t' = \gamma(t-\beta x) \text{ and } x' = \gamma(x-\beta t) \qquad \text{where } \beta = \frac{v}{c}. \tag{1.2}$$

In special relativity, all observers agree on not only the speed of light, but also the proper distance[7] given by,

$$ds^2 = \eta_{\mu\nu} dx^u dx^v = -dt^2 + dx^2 + dy^2 + dz^2, \tag{1.3}$$

where $\eta_{\mu\nu}$ is the Minkowski metric of flat spacetime. Lorentz transformations on the proper distance are invariant where $ds^2 > 0$ is spacelike and is casually connected, $ds^2 < 0$ is timelike and is casually connected and $ds^2 = 0$ is timelike and describes possible photon paths [7]. Soon after the formulation of special relativity, Albert Einstein comes up with the unified notion of gravity as a geometric property of space and time in a way to combine special relativity and Newton's law of universal gravitation called general relativity [10]. In general relativity, Einstein states that gravitational mass is equivalent to inertial mass, and that an accelerated system is indistinguishable to a system in a gravitational field [11].

1.2 The Metric Tensor and Geometry

Where special relativity placed no preference on any *one* inertial reference frame, general relativity abolished the need for a preference by showing that there is no preferred reference frame for the laws of nature at all [7]. Einstein states that all precise numerical quantities made from measurements depend on which coordinate system

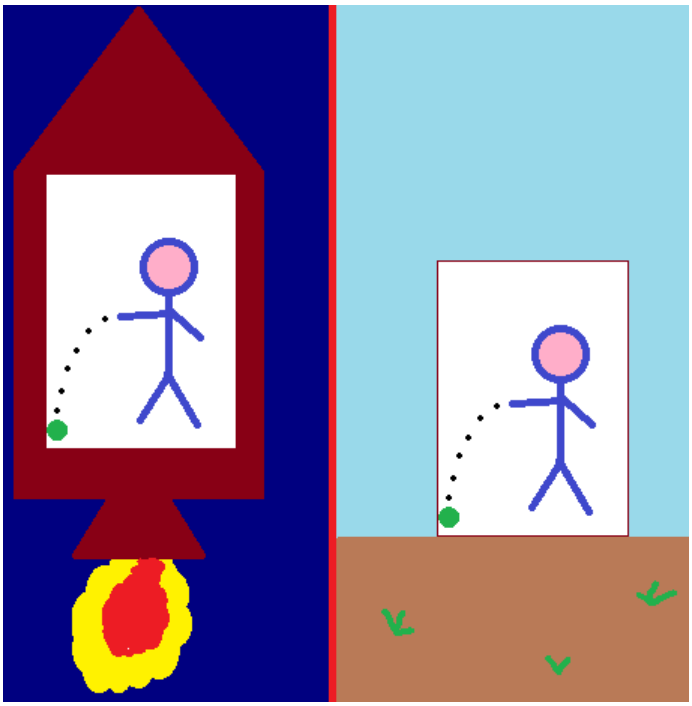

Figure 1: demonstrates the equivalence principle; the observer cannot distinguish between being on the surface of the earth and being in a spaceship accelerating in space at 1g. (Assuming the spaceship is small enough that differential tidal forces are negligible)

was used by the observer who made the measurements [11]. Thus to represent this mathematically, Einstein required the use of invariant objects, that are independent of the coordinate system, which can only be tensors [12]. In general relativity, the metric tensor is what determines the local geometry of spacetime and is given by [13]

$$ds^2 = g_{\mu\nu} dx^\mu dx^\nu \tag{1.4}$$

where the metric tensor, $g_{\mu\nu}$, has 10 independent components, since the tensor is symmetric, $g_{\mu\nu} = g_{\mu\nu}$ [13]. To follow convention, Greek indices go from 0-3 for one time and three spatial dimensions, and Latin indices go from 1-3 for the three spatial dimensions. In addition, the Einstein summation convention was followed where repeated upper and lower indices are to be summed together [7]. The metric can sometimes be considered to be representation of the gravitational potential when in a weak-field approximation [14].

1.2.1 Vectors

In Riemannian geometry, (tangent basis) vectors are defined via arguments about tangent spaces [15]:

$$(\vec{V} \cdot \nabla) f = V^{\mu} \frac{\partial}{\partial x^{\mu}} f \ . \tag{1.5}$$

If we change our coordinates to a different set of coordinates, designated by the prime, then we need to do a vector transformation. Remembering that the value of the operator has to remain invariant, we arrive at

$$V^{\nu\prime} \frac{\partial}{\partial x^{\nu\prime}} f = V^{\nu\prime} \frac{\partial x^{\mu}}{\partial x^{\nu\prime}} \frac{\partial}{\partial x^{\mu}} f. \tag{1.6}$$

Thus we arrive at our definition of a vector [11]

$$V^{\mu} = V^{\nu'} \frac{\partial x^{\mu}}{\partial x^{\nu'}}. \tag{1.7}$$

The transformation property of an object when we change the coordinates is what defines a vector. This transformation law also applies to displacements as well[16]

$$dx^{\mu} = dx^{\nu'} \frac{\partial x^{\mu}}{\partial x^{\nu'}}. \tag{1.8}$$

1.2.2 Covariant Vectors and Tensors

There are a number of objects that operate linearly on vectors. These includes operators such as gradients [17],

$$\partial_{\mu} \equiv \frac{\partial}{\partial x^{\mu}} = \frac{\partial x^{\nu'}}{\partial x^{\mu}} \frac{\partial}{\partial x^{\nu'}} = \frac{\partial x^{\nu'}}{\partial x^{\mu}} \partial \nu'. \tag{1.9}$$

If we call

$$\Lambda^{\nu'}{}_{\mu} \equiv \frac{\partial x^{\nu'}}{\partial x^{\mu}} \quad , \tag{1.10}$$

then we can say:

$$\partial_{\mu} = \Lambda^{\nu'}{}_{\mu} \partial \nu' \tag{1.11}$$

where $\Lambda^{\nu'}{}_{\mu}$ is a covariant tensor and can do the same transformations as gradients. With the use of tensors, we can transform each index individually when we change the coordinates. For example, the metric tensor, which is a linear operator acting on two vectors, can transform vectors much like a dot-product [16]

$$ds^2 = g_{\mu\nu} dx^{\mu} dx^{\nu} = g_{\mu\nu} \left(\frac{\partial x^{\mu}}{\partial x^{\alpha'}} dx^{\alpha'} \right) \left(\frac{\partial x^{\nu}}{\partial x^{\beta'}} dx^{\beta'} \right) = g_{\alpha'\beta'} dx^{\alpha'} dx^{\beta'} \tag{1.12}$$

and we find

$$g_{\alpha'\beta'} = g_{\mu\nu}\frac{\partial x^{\mu}}{\partial x^{\alpha'}}\frac{\partial x^{\nu}}{\partial x^{\beta'}} \leftrightarrow g_{\mu\nu} = g_{\alpha'\beta'}\frac{\partial x^{\alpha'}}{\partial x^{\mu}}\frac{\partial x^{\beta'}}{\partial x^{\nu}}. \tag{1.13}$$

The equation above shows the process of recalculating the metric when we change the coordinates.

1.2.3 Covariant Derivatives and Christoffel Symbols

When we take the partial derivatives of tensors, we do not get a tensor, as demonstrated [11]:

$$\frac{\partial}{\partial x^{\mu'}}T_{\nu'} = \frac{\partial x^{\mu}}{\partial x^{\mu'}}\frac{\partial}{\partial x^{\mu}}\left(\frac{\partial x^{\nu}}{\partial x^{\nu'}}T_{\nu}\right) = \frac{\partial x^{\mu}}{\partial x^{\mu'}}\frac{\partial x^{\nu}}{\partial x^{\nu'}}\left(\frac{\partial}{\partial x^{\mu}}T_{\mu}\right) + T_{\nu}\frac{\partial x^{\mu}}{\partial x^{\mu'}}\frac{\partial}{\partial x^{\mu}}\frac{\partial x^{\nu}}{\partial x^{\nu'}} \tag{1.14}$$

where the first term looks like a tensor, but the second term, which contains the derivatives of the change in coordinates, is not a tensor. Conveniently, there exists the differential operator called the covariant derivative, which accounts for the change in the vector field as well as taking into account the change in coordinates [18]. The covariant derivative can be defined as follows

$$\nabla_{\mu'}T_{\nu'} = \frac{\partial}{\partial x^{\mu'}}T_{\nu'} - \Gamma^{\alpha'}{}_{\mu'\nu'}T_{\alpha'} \tag{1.15}$$

where the Christoffel symbol, $\Gamma^{\alpha'}_{\mu'\nu'}$, is a new object constructed from the metric and its first derivatives that captures the coordinate derivatives like so [11]

$$\Gamma^{\alpha}{}_{\beta\gamma} = \tfrac{1}{2} g^{\alpha\sigma} \left(\partial_\beta g_{\gamma\sigma} + \partial_\gamma g_{\beta\sigma} - \partial_\sigma g_{\beta\gamma}\right). \tag{1.16}$$

1.2.4 Geodesics and Parallel Transport

To move a vector V^μ along the path of $x^\mu(t)$, while keeping it constant, let us introduce the notion of parallel transport [11]. In curved spacetime, the result of parallel transporting a vector from one point to another will depend on the path taken between the points [16]. In addition, parallel transport leaves the length of the vector invariant. The equation for parallel transport for a vector takes the form [14]:

$$\frac{d}{dt} V^\mu + \Gamma^{\mu}{}_{\sigma\rho} \frac{dx^\sigma}{dt} V^\rho = 0. \tag{1.17}$$

With the concept of parallel transport on our belts, we can then talk about geodesics, which is the path of the extremal distance between two points, or a path that parallel

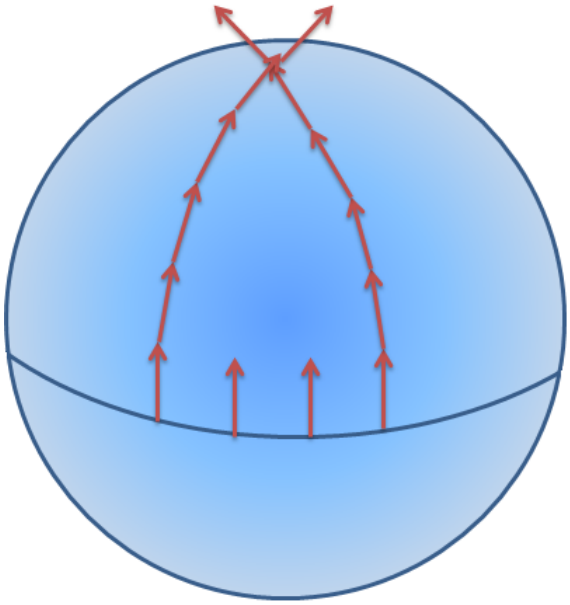

Figure 2: demonstrates the concept of parallel transport; on a curved surface like a sphere, the result of vector after being parallel transported depends on the path taken

transports its own tangent vector. Geodesics can also be considered as a curve whose tangent vector is parallel transported [11].

Given a path x^μ with its tangent vector dx^μ/dt, then its geodesic equation can be written as [11]

$$\frac{d^2x^\mu}{dt^2} + \Gamma^\mu{}_{\rho\sigma}\frac{dx^\rho}{dt}\frac{dx^\sigma}{dt} = 0. \tag{1.18}$$

1.3 Riemann Tensor, Ricci Tensor, and the Ricci Scalar

Suppose a vector in Minkowski space is parallel transported around a loop, the vector will point in the same direction it began after returning to its original position. In the more general case of curved space, this property does not hold [19]. Conveniently, there exists a tensor that details how the vector changes when it comes back to its initial point called the Riemann curvature tensor [11]. The Riemann tensor details the resulting transformation of this vector based on the total curvature enclosed by the loop at each point [11]. The Riemann tensor can be constructed through [14]:

$$R^{\rho}{}_{\sigma\mu\nu} = \partial_{\mu}\Gamma^{\rho}{}_{\nu\sigma} - \partial_{\nu}\Gamma^{\rho}{}_{\mu\sigma} + \Gamma^{\rho}{}_{\mu\lambda}\Gamma^{\lambda}{}_{\nu\sigma} - \Gamma^{\rho}{}_{\nu\lambda}\Gamma^{\lambda}{}_{\mu\sigma} \tag{1.19}$$

The Riemann tensor measures the extent to which the metric tensor is not locally flat for every point in space, and the curvature vanishes if and only if the spacetime is flat [11]. There exists symmetries in the Riemann tensor such as [14]:
being anti-symmetric in its first two indices

$$R_{\rho\sigma\mu\nu} = -R_{\sigma\rho\mu\nu}, \tag{1.20}$$

being anti-symmetric in its last two indices

$$R_{\rho\sigma\mu\nu} = -R_{\rho\sigma\nu\mu}, \tag{1.21}$$

and being symmetric upon the switching of the first and second pair of indices

$$R_{\rho\sigma\mu\nu} = R_{\mu\nu\rho\sigma}. \tag{1.22}$$

In addition, the sum of the cyclic permutations of the last three indices is zero,

$$R_{\rho\sigma\mu\nu} + R_{\rho\nu\mu\sigma} + R_{\rho\mu\sigma\nu} = 0 \quad . \tag{1.23}$$

With all the symmetries, when we perform the only possible contraction on the Riemann tensor, we will arrive at the Ricci tensor [17]

$$R_{\mu\nu} = R^{\lambda}{}_{\mu\lambda\nu} = R_{\nu\mu} \tag{1.24}$$

which is also symmetric from the symmetries of the Riemann tensor.

By taking another contraction, we can then define the Ricci scalar or the curvature scalar as [20],

$$R = R^{\nu}{}_{\nu} = g^{\mu\nu} R_{\mu\nu}. \tag{1.25}$$

Having defined the Ricci tensor and scalar, which encapsulates all the information about the traces of the Riemann tensor, we can then introduce the Weyl tensor [11]. The Weyl tensor contains the trace-free parts of the Riemann Tensor (with all of its contractions removed) and still keeps all of the symmetries of the Riemann tensor [14] [21]:

$$C^{\mu\nu}{}_{\rho\sigma} = R^{\mu\nu}{}_{\rho\sigma} - 2\delta^{[\mu}{}_{[\rho} R^{\nu]}{}_{\sigma]} + \frac{1}{3}\delta^{[\mu}{}_{[\rho}\delta^{\nu]}{}_{\sigma]} R \tag{1.26}$$

where $\delta^{\mu}{}_{\rho}$ is the Kronecker delta, and the square brackets indicate antisymmetrization.

In vacuum spacetime, the Weyl tensor is equivalent to the Riemann curvature tensor, $C^{\mu\nu}{}_{\rho\sigma} = R^{\mu\nu}{}_{\rho\sigma}$, thus the Weyl tensor contains all information about spacetime

curvature [21].

1.4 Einstein Equations

The Einstein field equations are a set of 10 nonlinear coupled partial differential equations in Albert Einstein's general theory of relativity which describe the fundamental interaction of gravitation as a result of spacetime being curved by matter and energy[17]. Energy, momentum, and stress of matter are all represented by the stress-energy tensor T^{ab}[22]. The Einstein's field equations relate the geometry of spacetime to the local matter content in the Universe according to [14]

$$G_{ab} = 8\pi T^{ab}, \tag{1.27}$$

where G_{ab} is the symmetric Einstein tensor defined by the Ricci tensor and scalar

$$G_{ab} = R_{ab} - \frac{1}{2} g_{ab} R = 8\pi T^{ab}. \tag{1.28}$$

It is this equation that describes how the curvature of the spacetime reacts to the presence of energy and momentum [20]. As Wheeler saids it, "matter tells how space-

time should curve, and spacetime tells matter how to move" [14]. Moreover, gravity curves the trajectories of objects, towards the gravitating mass-energy, and orbiting bodies think they are traveling in straight paths [7]. Being nonlinear and coupled, the Einstein field equations are very difficult to solve analytically, except for the special cases of the stationary black hole. Solving for the more complex cases such binary black hole mergers can only be done numerically with the use of supercomputers [22].

1.5 Schwarzschild Metric

The most familiar black hole solution is the stationary Schwarzschild black hole where there is neither charge nor angular momentum [7]. The Schwarzschild metric is as follows [14]:

$$ds^2 = -\left(1 - \frac{2GM}{r}\right) dt^2 + \left(1 - \frac{2GM}{r}\right)^{-1} dr^2 + r^2 d\Omega^2 \tag{1.29}$$

where $d\Omega^2 = d\theta^2 + sin^2\theta d\phi^2$ and c=1.

Notice how at r=2M, the radial term blows up. This is the Schwarzschild radius or the event horizon, where light cannot escape. This is however, a coordinate singularity, because it is only an artifact of the coordinates we chose, for example, if we just let

$$R = \tfrac{1}{2}(r - M + \sqrt{r(r-2M)}) \quad , \tag{1.30}$$

then we find that the metric takes the isotropic form [20]:

$$ds^2 = -\left(\frac{1 - M/2R}{1 + M/2R}\right)^2 dt^2 + \left(1 + \frac{M}{2R}\right)^4 (dR^2 + r^2 d\Omega^2) \tag{1.31}$$

and thus we have successfully removed the r=2M singularity. However, there still exists the real singularity at r=0, which cannot be removed because our description of the manifold at this point is ill-defined. [11]

1.6 Linearized Gravity and Gravitational Radiation

In places not near the strong-gravity regions of black holes or neutron stars, curvature is not so extreme. In these cases, we are safe to assume linearized gravity with rectangular coordinates and metric perturbations [14]:

$$g_{\mu\nu} = \eta_{\mu\nu} + h_{\mu\nu} \tag{1.32}$$

where $h_{\mu\nu}$ is a small perturbation to the Minkowski flat spacetime, $h_{\mu\nu} \ll 1$ In this proper gauge, we can reduce Einstein's equations to the form [14]:

$$\Box h_{\mu\nu} = \left(-\partial_t^2 + \nabla^2\right) h = -16\pi G T_{\mu\nu} \tag{1.33}$$

where $\Box$ is the flat-space wave operator.

This is the wave equation which predicts the existence of gravitational waves. It can be shown that they are transverse, like EM waves, but with only two polarizations [22].

2 Gravitational Waves and their detection

Predicted to exist by Albert Einstein on the basic of his theory of general relativity, gravitational waves theoretically transport energy as gravitational radiation. A theory that is consistent with special relativity means that changes in the gravitational field cannot occur everywhere simultaneously; they must propagate at the speed of light [22]. The sources of gravitational waves are large mass bodies, as opposed to the atomic level in electromagnetic radiation. By studying the emitting gravitational radiation from large-bodies, we can gain better insight of the most fascinating physical phenomena in the Universe - black holes, supernovas, neutrons stars, and galaxy

collisions [23]. In addition, gravitational waves can pass through any intervening matter without being scattered significantly [23]. And as a gravitational wave passes a distant observer, that observer will find spacetime distorted by the effects of strain [22]. These effects caused by gravitational waves are extremely difficult to measure as the waves are several orders of magnitude smaller than the hydrogen atom, thus very precise gravitational interferometers have been constructed in hopes to gain a better image of our universe through gravitational wave observations [24].

2.1 Sources

Generally, gravitational waves are radiated by objects whose motion involves acceleration, provided that the motion is not perfectly spherically symmetric or cylindrically symmetric [22]. Significant sources of gravitational waves include black hole mergers, rotating neutrons stars, and supernovas [22]. As these gravitational fields propagate away from their sources, however, they will reach an asymptotic region in which they can be modeled as a linear perturbation of a nearly Minkowski spacetime. These linearized gravitational waves carry information about the nature of the nonlinear sources that generated them [22]. It is these linearized waves that will be detected by our gravitational wave interferometers in the near future [22].

2.2 Numerical Relativity

Because the Einstein field equations are nonlinear coupled equations, we cannot easily solve them analytically besides the special cases. They must be solved numerically through the use of sophisticated algorithms on supercomputers [22]. Numerical relativity has allowed us to recreate cataclysmic cosmic phenomena, from gravitational collapse to black holes and neutron stars, the inspiral and coalescence of binary black

holes and neutron stars, and the generation and propagation of gravitational waves [11]. Numerical Relativity allows us to follow from linearized gravity to the nonlinear dynamics and relativistic instabilities and simulate the final state of these systems [11]. One of the current goals of numerical relativity now is the generation of waveforms from binary black hole mergers for identification and physical interpretation. This task is crucial as large libraries of numerical waveform templates are essential for analyzing the data from ground-based and space-borne laser interferometers [25].

3 Tendex and Vortex Lines

3.1 Newman-Penrose Formalism

In numerical relativity, there exist variables which can easily express the gravitational-wave content of many dynamical simulations far from the source. These variables are called the Weyl scalars which are formulated through the Newman-Penrose Formalism [6]. In order to reach the scalars, we first define an orthonormal tetrad $\vec{e}_{\hat{\alpha}} = (\vec{e}_{\hat{0}}, \vec{e}_{\hat{1}}, \vec{e}_{\hat{2}}, \vec{e}_{\hat{3}})$ with the time basis vector $\vec{e}_{\hat{0}} = \vec{u}$ orthogonal to the spacelike hypersurfaces, and with the spatial basis vectors $\vec{e}_{\hat{1}}$, $\vec{e}_{\hat{2}}$, $\vec{e}_{\hat{3}}$ lying in those hypersurfaces [21]. Using this tetrad, we can build a complex null tetrad for use in the NP formalism:

$$\vec{l} = 1/\sqrt{2}(\vec{e}_{\hat{0}} + \vec{e}_{\hat{1}}) \qquad \vec{n} = 1/\sqrt{2}(\vec{e}_{\hat{0}} - \vec{e}_{\hat{1}}) \tag{3.1}$$

$$\vec{m} = 1/\sqrt{2}(\vec{e}_{\hat{2}} + i\vec{e}_{\hat{3}}) \qquad \vec{m}^* = 1/\sqrt{2}(\vec{e}_{\hat{2}} - i\vec{e}_{\hat{3}}). \tag{3.2}$$

Projecting the Weyl tensor onto this null basis, we arrive at the complex Weyl Scalars [26],

$$\Psi_0 = C_{\mu\nu\rho\sigma} l^\mu m^\nu l^\rho m^\sigma \tag{3.3}$$

$$\Psi_1 = C_{\mu\nu\rho\sigma} l^\mu n^\nu l^\rho m^\sigma \tag{3.4}$$

$$\Psi_2 = C_{\mu\nu\rho\sigma} l^\mu m^\nu m^{*\rho} n^\sigma \tag{3.5}$$

$$\Psi_3 = C_{\mu\nu\rho\sigma} l^\mu n^\nu m^{*\rho} n^\sigma \tag{3.6}$$

$$\Psi_4 = C_{\mu\nu\rho\sigma} n^\mu m^{*\nu} n^\rho m^{*\sigma} \tag{3.7}$$

Using this null tetrad, which is transverse, the scalars Ψ_0 and Ψ_4 measure the ingoing and outgoing gravitational radiation, the scalars Ψ_1 and Ψ_3 vanish, and the scalar Ψ_2 is the longitudinal, or "Coulombic" part of the gravitational field [22].

3.2 Tendex and Vortex Lines

The Weyl tensor $C_{\mu\nu\rho\sigma}$ consists of two symmetric, traceless spatial tensors $\mathcal{E}$ and $\mathcal{B}$ [27]. These tensors are the gravitational analogs of the electric and magnetic fields in Maxwell's theory. The electric part $\mathcal{E}$, which is the tidal field in the Newtonian limit, handles the gravitational stretching and compressing that generates tides [28]. The magnetic part $\mathcal{B}$, which is the frame-drag field, describes the differential frame-dragging precession of spacetime [29]. The $\mathcal{E}$ and $\mathcal{B}$ tensors each have three orthogonal eigenvector fields which can be depicted by their integral curves. We call the integral

curves of $\mathcal{E}$'s eigenvectors tidal tendex lines, and these lines provide the preferred directions of strain at a point in spacetime. Following that, the eigenvalues, or the tendicity of a tendex line, gives the magnitude of the strain along the tendex lines. The integral curves of $\mathcal{B}$'s eigenvectors are the vortex lines, and they give the preferred directions of the differential precession of gyroscopes. The eigenvalues, or the vorticity of the vortex lines, gives the magnitude of the precession along the vortex lines [28].

These lines allow us to understand the nonlinear dynamics of curved spacetime. The tidal field $\mathcal{E}$ describes the local tidal forces between nearby points in spacetime, and the frame-drag field $\mathcal{B}$ describes the relative precession of nearby gyroscopes. In a Lorentz frame of two freely falling observers who are separated by a spatial vector ξ^j, the differential acceleration experienced by the observers is [6]

$$\Delta a^i = -\mathcal{E}^i_j \xi^j. \tag{3.8}$$

If the two same observers carry inertial gyroscopes, each will measure the gyroscope of the other to precess with an angular velocity by $\mathcal{B}$ relative to their own by [21],

$$\Delta \Omega^i = -\mathcal{B}^i_j \xi^j. \tag{3.9}$$

If two observers have a small separation along a tendex line, they will experience an acceleration along that line with a magnitude given by the eigenvalue or tendicity of that tendex line. In the same way, the two observers separated along a vortex line will experience differential frame dragging with a magnitude given by the eigenvalue or vorticity of that vortex line [21].

To find $\mathcal{E}_{ij}$ and $\mathcal{B}_{ij}$ tensors, we first split the Weyl tensor covariantly into two irreducible parts, which are symmetric, trace-free, and lie in the foliation's hyperspaces (orthogonal to u^{μ}) like so [21]

$$\mathcal{E}_{ij} = C_{i\hat{0}j\hat{0}}, \tag{3.10}$$

and

$$\mathcal{B}_{ij} = \frac{1}{2}\epsilon_{ipq}C^{pq}. \tag{3.11}$$

where the indices are components in the reference frame of "orthogonal observers" who move orthogonal to the spatial slices, $\hat{0}$ is their time component, and ϵ_{piq} is their spatial Levi-Civita tensor.

Using the null tetrad built from our orthonormal tetrad, we can write the spatial or-

thonormal components of the electric and magnetic parts of the Weyl tensor in terms of Weyl scalars as follows [21]:

$$\mathcal{E}_{\hat{a}\hat{b}} + i\mathcal{B}_{\hat{a}\hat{b}} = \begin{bmatrix} 2\Psi_2 & -(\Psi_1 - \Psi_3) & i(\Psi_1 + \Psi_3) \\ * & \frac{\Psi_0+\Psi_4}{2} - \Psi_2 & -\frac{i}{2}(\Psi_0 - \Psi_4) \\ * & * & -\frac{\Psi_0+\Psi_4}{2} - \Psi_2 \end{bmatrix} \tag{3.12}$$

where * components are given by the symmetry of the tensor. By using the Weyl scalars, we are actually using variables that describe gravitational radiation far from the source in order to study the strong-gravity regions near black holes.

4 Implementation

4.1 Equations

Using the Weyl tensor, the individual elements of the $\mathcal{E}$ and $\mathcal{B}$ tensors were derived from Eq. 3.10 and 3.11. We solved each tensor in terms of Weyl scalars like so in Eq. 3.12. Furthermore, the Weyl scalars were also separated in terms of the real and imaginary components in each tensor component.

$$\mathcal{E}_{\hat{1}\hat{1}} = R_{\hat{1}\hat{0}\hat{1}\hat{0}} = R_{ijkm} e_1^i e_0^j e_1^k e_0^m \tag{4.1}$$

Next, we can rewrite each of the orthonormal tetrads in terms of the complex null tetrads.

$$\vec{e}_0 = \frac{k}{2}(\vec{l} + \vec{n}) \qquad \vec{e}_2 = \frac{k}{2}(\vec{m} + \vec{m^*}) \tag{4.2}$$

$$\vec{e}_1 = \frac{k}{2}(\vec{l} - \vec{n}) \qquad \vec{e}_2 = \frac{k}{2}(\vec{m} - \vec{m^*}) \tag{4.3}$$

We can rewrite the first component of the electric tensor as

$$R_{\hat{1}\hat{0}\hat{1}\hat{0}} = \frac{k^4}{16} R_{ijkm}(\vec{l} - \vec{n})^i(\vec{l} + \vec{n})^j(\vec{l} - \vec{n})^k(\vec{l} + \vec{n})^m. \tag{4.4}$$

Expanding the equation above completely yields

$$\mathcal{E}_{\hat{1}\hat{1}} = \frac{k^4}{16} R_{ijkm}(\vec{l} - \vec{n})^i(\vec{l} + \vec{n})^j(\vec{l} - \vec{n})^k(\vec{l} + \vec{n})^m = \frac{k^4}{16}[R_{llll} + R_{llln} - R_{llnl} - R_{llnn} + R_{lnll} + R_{lnln} - R_{lnnl} - R_{lnnn} - R_{nlll} - R_{nlln} + R_{nlnl} + R_{nlnn} - R_{nnll} + R_{nnln} + R_{nnnl} + R_{nnnn}].$$

Using some symmetry properties of the Riemann tensor such as Eq. 1.22, 1.23, and 1.24 where the Riemann tensor is anti-symmetric in its first two and last two indices and invariant under the switching of the first and last pair of indices allows us to simplify the long-expression above. In addition, using the identity from Eq. 1.25 where the Riemann tensor's sum of cyclic permutations of the last three indices is zero [11] leaves us with

$$\frac{k^4}{16} R_{lnln}. \tag{4.5}$$

This still isn't any of the Weyl scalars, but we can do:

$$\frac{k^4}{16} R_{lnln} = g^{nl} R_{lnln} = -R^n_{nln} = R^n_{nnl} = -(R^l_{nll} + R^m_{nml} + R^{m^*}_{nm^*l}) \tag{4.6}$$

where we used the fact that the Ricci tensor vanishes in vacuum spacetimes.

$$R_{nl} = R^l_{nll} + R^n_{nnl} + R^m_{nml} + R^{m^*}_{nm^*l} = 0 \ . \tag{4.7}$$

We can also prove that $R^l_{nll} = 0$ in Eq. 4.9 by first lowering the indices using the metric,

$$g_{\alpha\beta} = g^{\alpha\beta} = \begin{pmatrix} 0 & -1 & 0 & 0 \\ -1 & 0 & 0 & 0 \\ 0 & 0 & 0 & 1 \\ 0 & 0 & 1 & 0 \end{pmatrix}. \tag{4.8}$$

and then using Bianchi's Second identity,

$$R^l_{nll} = g_{nl}R^l_{nll} = R^{nnll} = -R_{nlln} - R_{nlnl} = 0. \tag{4.9}$$

So we are now left with,

$$-R^m_{nml} - R^{m^*}_{nm^*l} = -g_{m^*m}R^m_{nml} - g_{mm^*}R^{m^*}_{nm^*l} = -R_{m^*nml} - R_{mnm^*l} = R_{lmm^*n} + R_{lm^*mn} \tag{4.10}$$

Comparing the last expression to our expressions for the Weyl scalars in Eq. 3.3

to 3.7, we arrive at:

$$\mathcal{E}_{\hat{1}\hat{1}} = \Psi_2 + \Psi_2^*, \tag{4.11}$$

which is successfully written in terms of the real and imaginary components of the Weyl scalar, Ψ_2. Doing the same for the magnetic tensor gives:

$$\mathcal{B}_{\hat{1}\hat{1}} = \frac{1}{2}\epsilon_{\hat{1}}^{\hat{p}\hat{q}} R_{\hat{p}\hat{q}\hat{1}\hat{0}} = \frac{1}{2}(\epsilon_{\hat{1}}^{\hat{2}\hat{3}} R_{\hat{2}\hat{3}\hat{1}\hat{0}} - \epsilon_{\hat{1}}^{\hat{3}\hat{2}} R_{\hat{3}\hat{2}\hat{1}\hat{0}}) \tag{4.12}$$

where we followed the normalization for the Levi-Civita tensor in a right-handed orthonormal frame, $\epsilon_{\hat{0}\hat{1}\hat{2}\hat{3}} = +1$ and is defined by $\epsilon_{\hat{i}\hat{p}\hat{q}} = \epsilon_{\hat{0}\hat{i}\hat{p}\hat{q}}$ with $\epsilon_{\ \hat{1}\hat{2}\hat{3}} = 1$ in a right-handed orthonormal basis.

Using some symmetries of the Riemann curvature tensor yields

$$\frac{1}{2}(R_{\hat{2}\hat{3}\hat{1}\hat{0}} - R_{\hat{3}\hat{2}\hat{1}\hat{0}}) = \frac{1}{2}(R_{\hat{2}\hat{3}\hat{1}\hat{0}} + R_{\hat{2}\hat{3}\hat{1}\hat{0}}) = R_{\hat{2}\hat{3}\hat{1}\hat{0}}\ . \tag{4.13}$$

Transforming the orthonormal basis to our null basis gives

$$R_{\hat{2}\hat{3}\hat{1}\hat{0}} = \frac{k^4}{16i} R_{\hat{2}\hat{3}\hat{1}\hat{0}} (\vec{m} + \vec{m^*})^{\hat{2}} (\vec{m} - \vec{m^*})^{\hat{3}} (\vec{l} - \vec{n})^{\hat{1}} (\vec{l} + \vec{n})^{\hat{0}}. \tag{4.14}$$

Symmetries once again will yield us

$$\frac{k^4}{16i}(-R_{mm^*ln} + R_{mm^*nl} + R_{m^*mln} - R_{m^*mnl}) = \frac{ik^4}{4} R_{lnmm^*}. \tag{4.15}$$

Using Bianchi's second identity again gives:

$$\frac{ik^4}{4} R_{lnmm^*} = \frac{ik^4}{4}(-R_{lmm^*n} - R_{lm^*nm}) = \frac{ik^4}{4}(-R_{lmm^*n} + R_{lm^*mn}) \ , \tag{4.16}$$

$$\mathcal{B}_{\hat{1}\hat{1}} = \frac{ik^4}{4}(-\Psi_2 + \Psi_2^*), \tag{4.17}$$

which is once again in terms of the real and imaginary components of the scalars. To check, we can sum the elements of $\mathcal{E}_{\hat{1}\hat{1}}$ and $\mathcal{B}_{\hat{1}\hat{1}}$, and we indeed arrive at the corresponding Weyl Tensor component with the scalar $2\Psi_2$ in Eq. 3.12.

We used the same approach to derive the rest of the real spatial tensors of $\mathcal{E}$ and $\mathcal{B}$ from slicings of the Weyl tensor in terms of Weyl scalars, and the following tensors were arrived:

$$\mathcal{E}_{\hat{a}\hat{b}} = \frac{k^4}{4}\begin{pmatrix} 2\mathbf{Re}\Psi_2 & (\mathbf{Re}\Psi_3 - \mathbf{Re}\Psi_1) & (-\mathbf{Im}\Psi_1 - \mathbf{Im}\Psi_3) \\ * & \frac{1}{2}(\mathbf{Re}\Psi_0 - 2\mathbf{Re}\Psi_2 + \mathbf{Re}\Psi_4) & \frac{1}{2}(\mathbf{Im}\Psi_0 - \mathbf{Im}\Psi_4) \\ * & * & \frac{1}{2}(-\mathbf{Re}\Psi_0 - 2\mathbf{Re}\Psi_2 - \mathbf{Re}\Psi_4) \end{pmatrix} \tag{4.18}$$

$$\mathcal{B}_{\hat{a}\hat{b}} = \frac{k^4}{4}\begin{pmatrix} 2\mathbf{Im}\Psi_2 & (\mathbf{Im}\Psi_3 - \mathbf{Im}\Psi_1) & (\mathbf{Re}\Psi_1 + \mathbf{Re}\Psi_3) \\ * & \frac{1}{2}(\mathbf{Im}\Psi_0 - 2\mathbf{Im}\Psi_2 + \mathbf{Im}\Psi_4) & \frac{1}{2}(-\mathbf{Re}\Psi_0 + \mathbf{Re}\Psi_4) \\ * & * & \frac{1}{2}(-\mathbf{Im}\Psi_0 - 2\mathbf{Im}\Psi_2 - \mathbf{Im}\Psi_4) \end{pmatrix} \tag{4.19}$$

where * components are given by the symmetry of the tensor and k is some real constant.

4.2 Numerical Implementation

The real, symmetric matrices, $\mathcal{E}_{\hat{a}\hat{b}}$ and $\mathcal{B}_{\hat{a}\hat{b}}$ are completely characterized by their orthogonal eigenvectors and corresponding eigenvalues [6]. Note that, since each tensor is traceless, the sum of its three eigenvalues must vanish[6]. Our code for producing the field lines to visualize spacetime curvature is to find the eigenvector fields by solving the eigenvalue problem [5],

$$\mathcal{E}^i_j v^j = \lambda v^i \tag{4.20}$$

And the same eigenvalue problem is applied for the frame-drag field as well. This results in three eigenvectors fields for each of the two tensors, $\mathcal{E}_{\hat{a}\hat{b}}$ and $\mathcal{B}_{\hat{a}\hat{b}}$. These fields are vector fields on the spatial slice, and behave as usual under transformations of the spatial coordinates [27]. By integrating along these eigenvector fields, we arrive at a set of three tendex lines and three vortex lines [6]. At Georgia Tech, I used the Maya code which consists of the Einstein Toolkit which runs on a Cactus framework and Carpet mesh refinement. The Einstein toolkit is an open access code for use in numerical relativity and relativistic astrophysics simulations [30]. The Einstein toolkit simulates spacetime evolution through the BSSN evolution system and relativistic-hydrodynamics [30]. The toolkit's infrastructure is based on Cactus, which consists of the central component called the flesh, and it interacts with the modular components called thorns [30]. The flesh provides the variables and data types, the parameters, input/output, and etc. These thorns provide additional functionality [30]. I created a

thorn called EBWeyl that inputs the Weyl scalars that were calculated from another thorn called WeylScal4 and assembled the E and B tensors. I then have a loop over every grid point in the grid function that calculates the eigenvectors and eigenvalues using the GSL solver for real generalized symmetric-definite eigensystems.

4.3 Visualization

I implemented this thorn in three different scenarios: a stationary black hole of mass = 1 and radius of 0.5. A rotating black hole with mass = 1, radius of 0.5, and spin of (0,0,0.6), and a binary black hole system with equal masses of 0.5, and a radius of 0.25. Geometrized units were used where G = c = 1 and normalized to the mass of the system M, using the metric signature (-,+,+,+). The simulations outputted data in HDF5, which is a file format for datasets comprised of multidimensional arrays. The data was then inputted into the visualization software, VisIt, which numerically integrates along the eigenvectors to produce streamlines. In VisIt, the streamlines were created with starting points on a sphere of radius 0.5, centered at (0,0,0), with 35 uniformly spaced lines in the latitudinal and radial directions and 1 line along the longitudinal direction. The Runge-Kutta 4 algorithm was used to integrate along the vector fields to produce streamlines with a step length of 0.01 and with 1,000 steps. Below are a few selected frames from the visualization movies of the runs.

4.3.1 Schwarzschild Black Hole

For the stationary black hole case, the frame-drag field vanishes and the tidal field has degenerate eigenvalues.

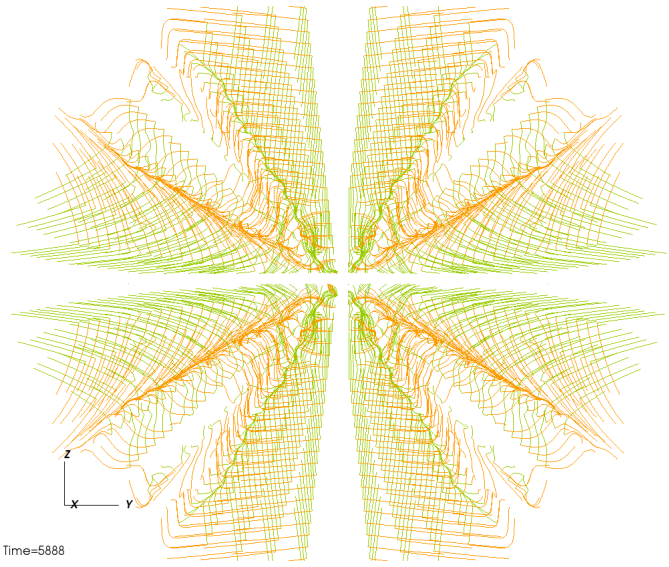

Figure 3: shows the tendex lines for a Schwarzschild black hole of mass 1.0: the blue (into the plane of the page), green, and orange lines represent the three orthogonal tendex lines

4.3.2 Kerr Black Hole

Now the black hole is given a spin of (0,0,0.6), and the degeneracy in the eigenvalues of the tidal field is broken. In addition, the slow rotation allows for the existence of the frame-drag field.

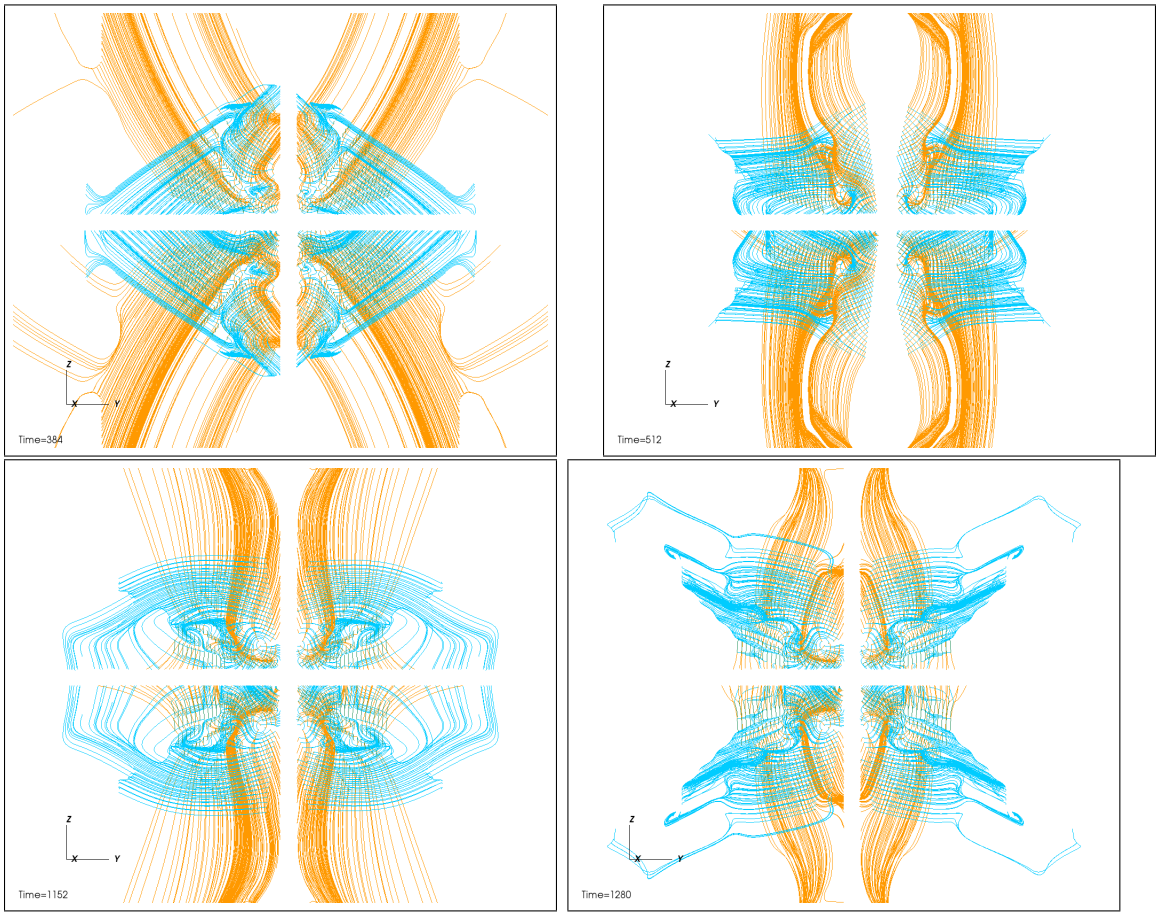

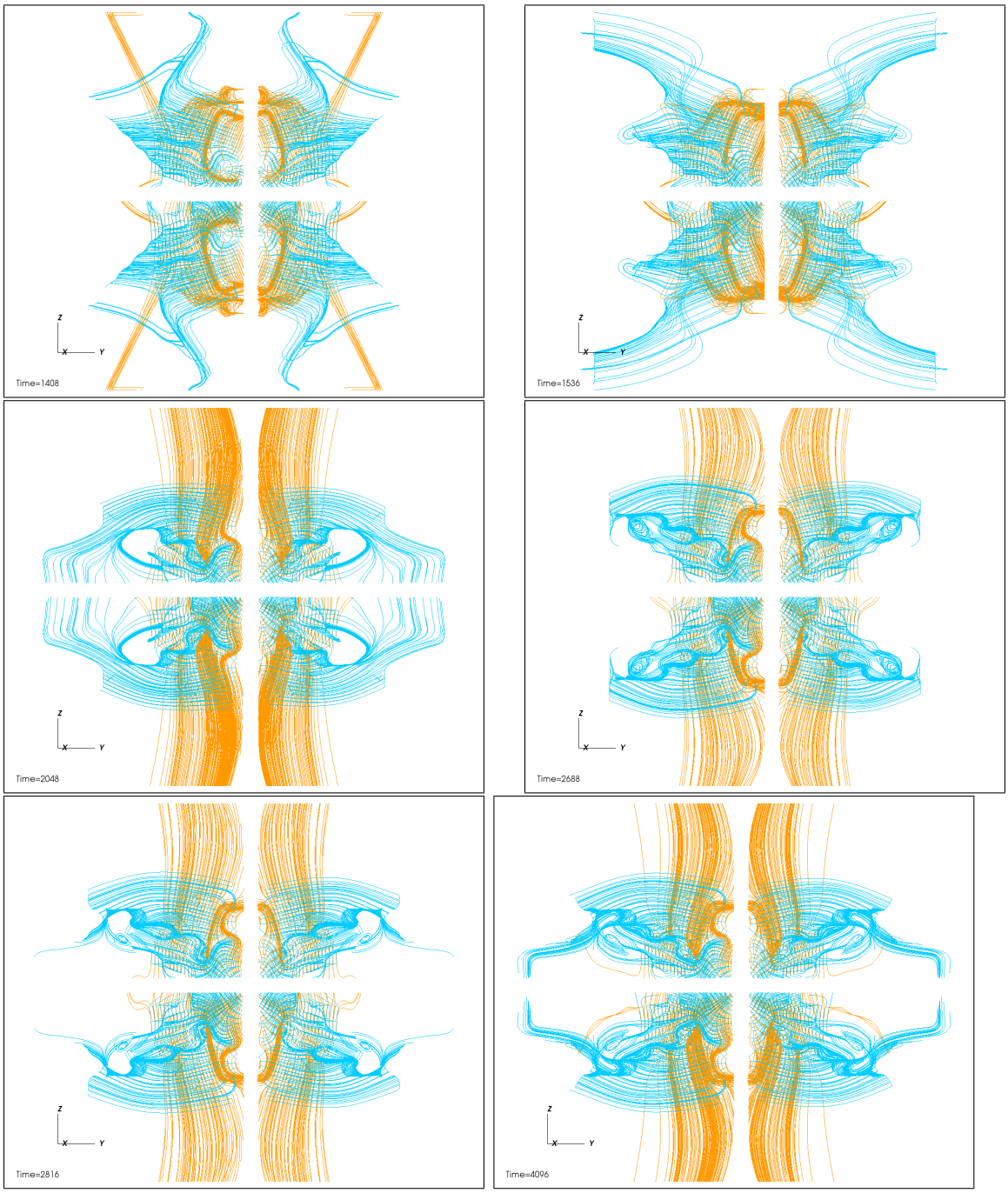

Figure 4: shows the vortex lines for a Kerr black hole of mass = 1.0 and spin of (0,0,0.6) at different time frames: the blue, green, and orange lines indicate the three orthogonal vortex lines

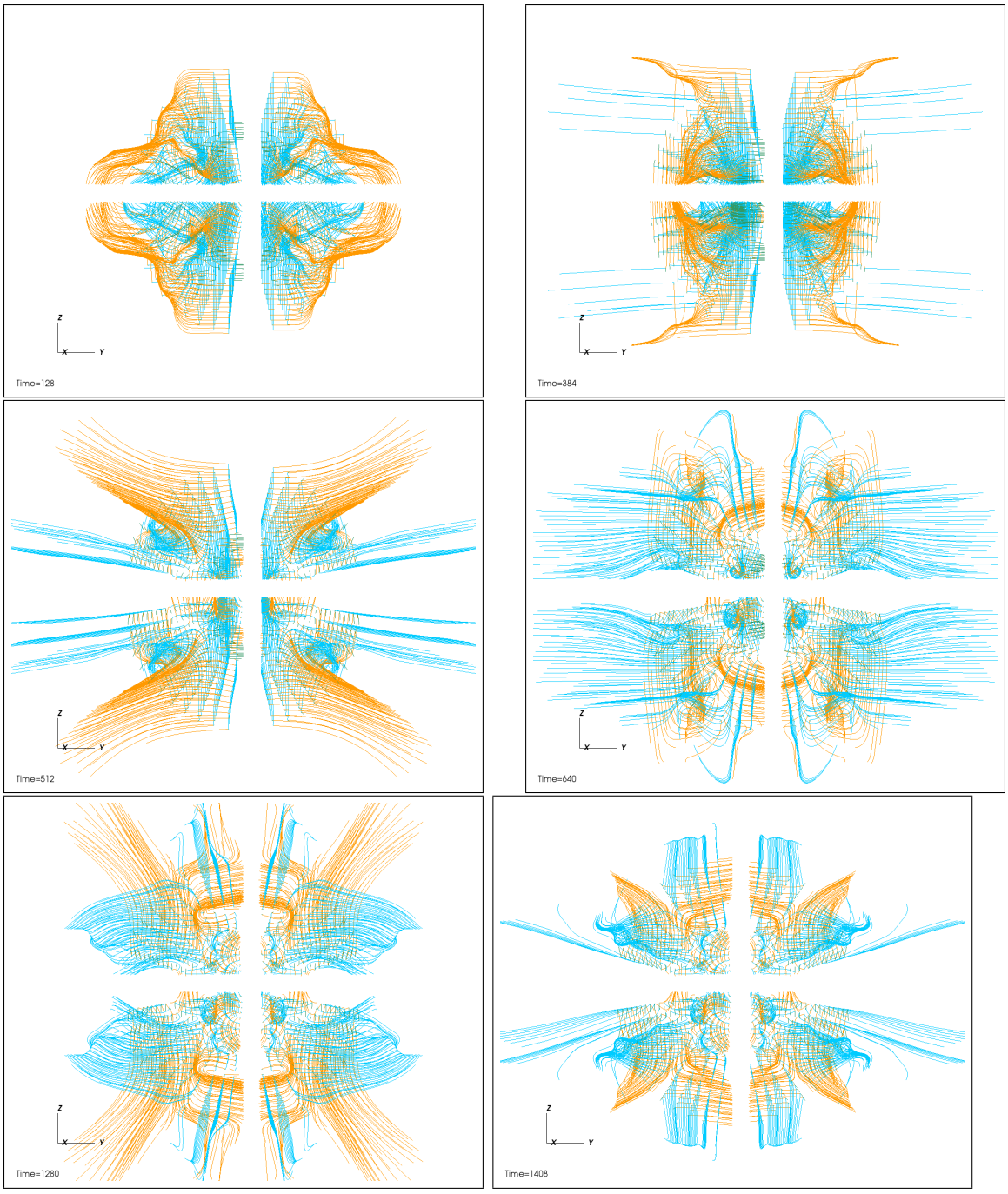
Time=128
Time=384
Time=512
Time=640
Time=1280
Time=1408

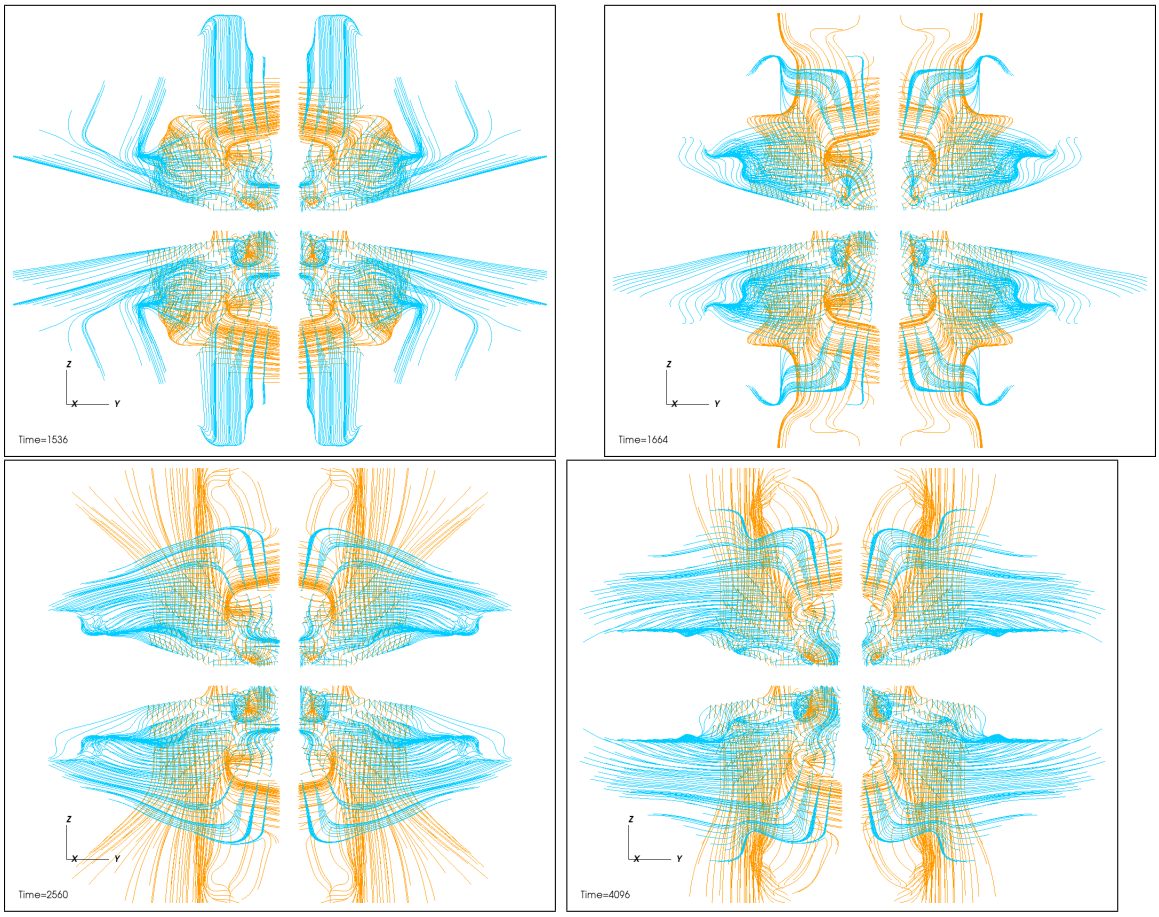

Figure 5: shows the tendex lines for a Kerr black hole of mass = 1.0 and spin of (0,0,0.6) at different time frames: the blue, green, and orange lines indicate the three orthogonal tendex lines

4.3.3 Binary Black Hole Merger

For the binary black hole merger, equal mass black holes with equal masses of 0.5 were placed 2.32 away from each other initially.

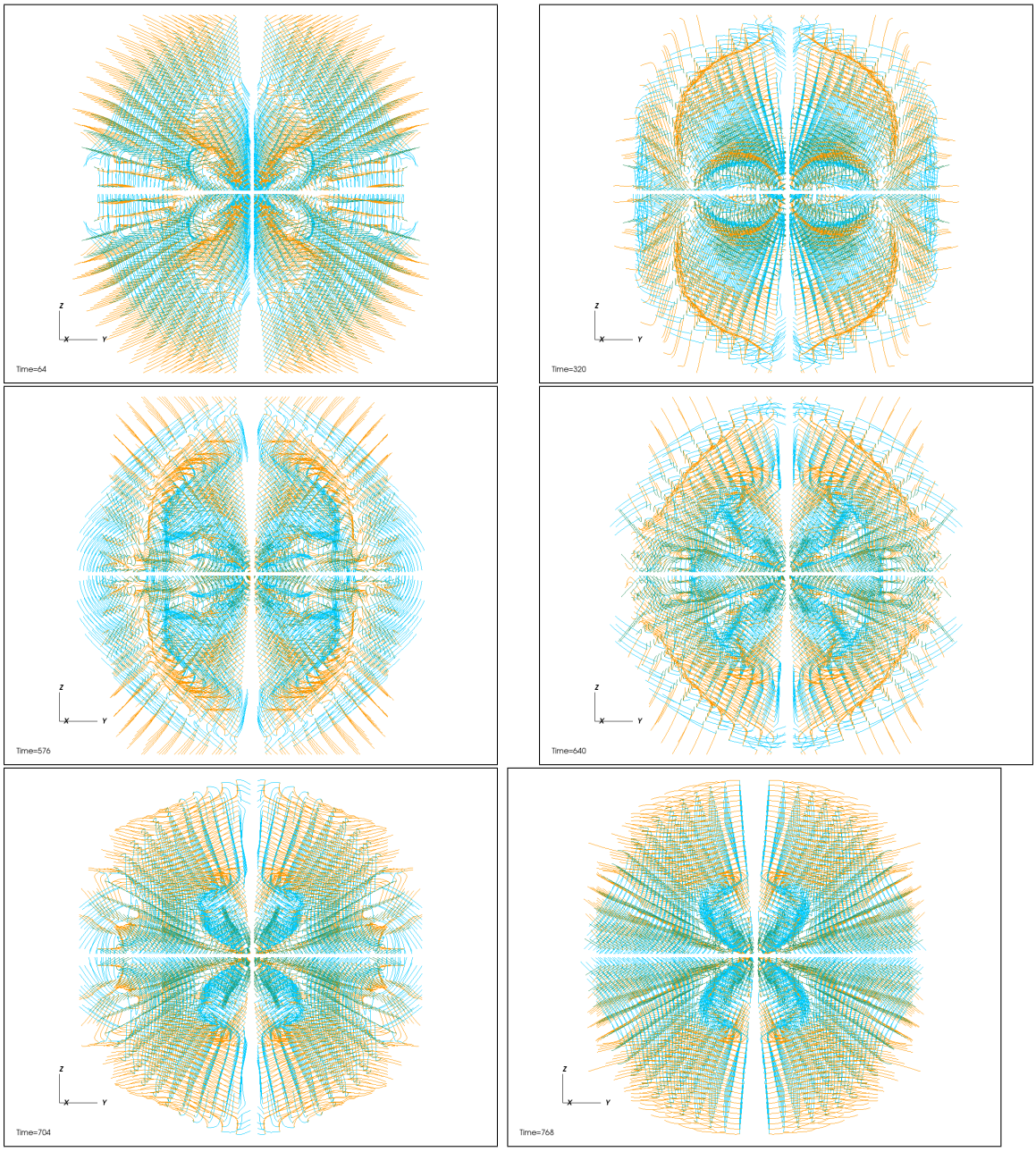
Z
X
Y
Time=64
Time=320
Time=576
Time=640
Time=704
Time=768

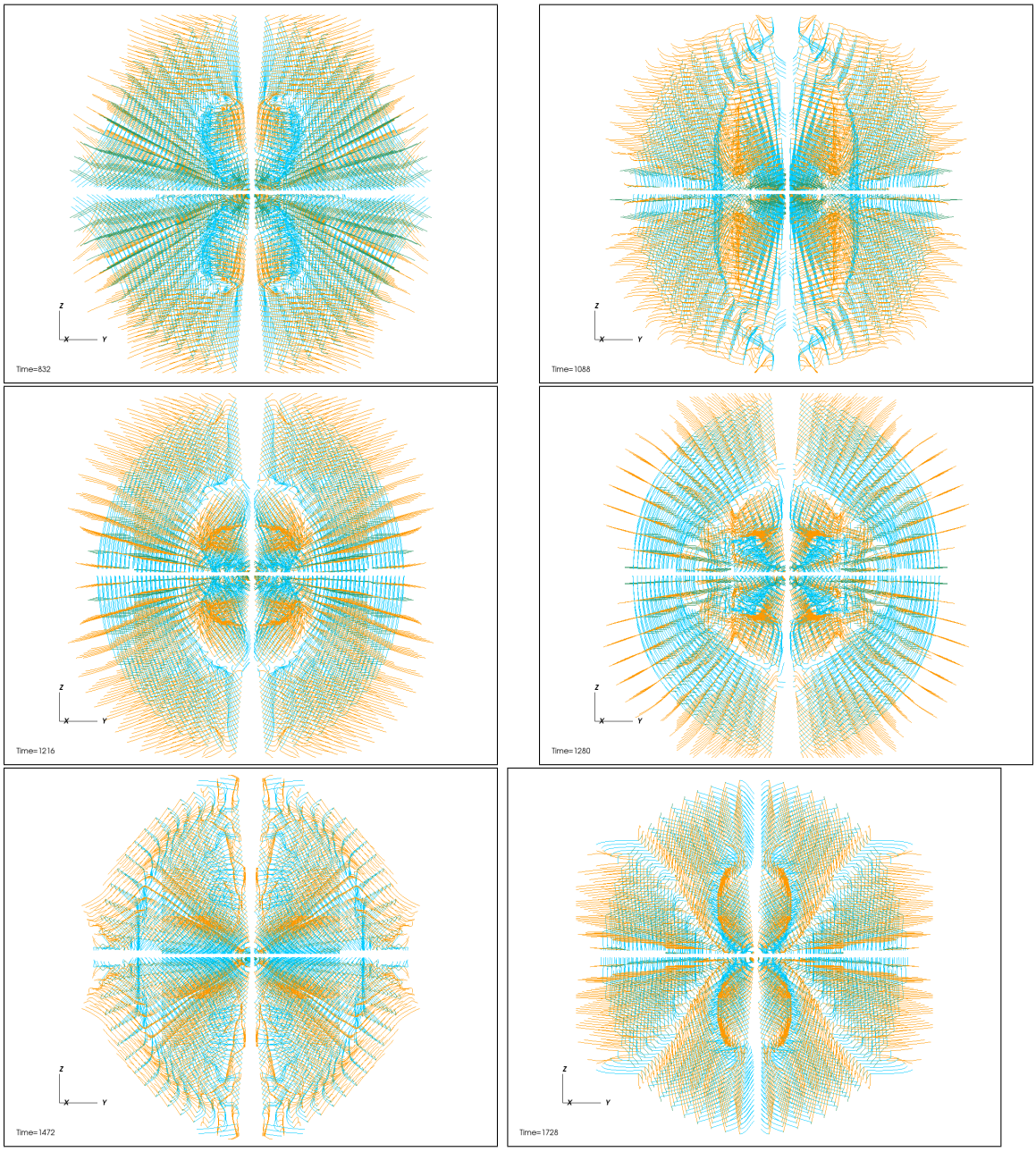
Z
X
Y
Time=832
Time=1088
Time=1216
Time=1280
Time=1472
Time=1728

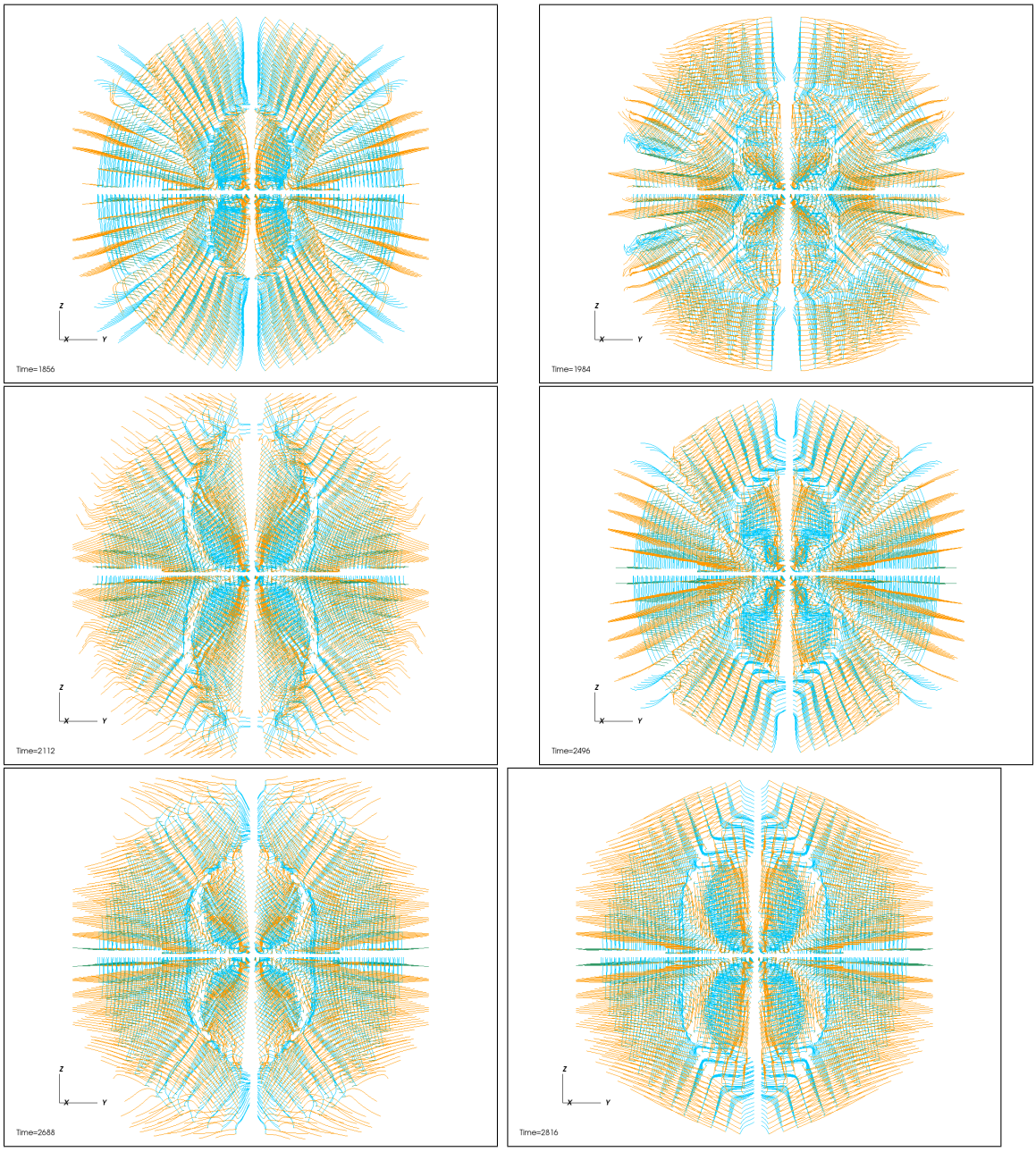
Time=1856
Time=1984
Time=2112
Time=2496
Time=2688
Time=2816

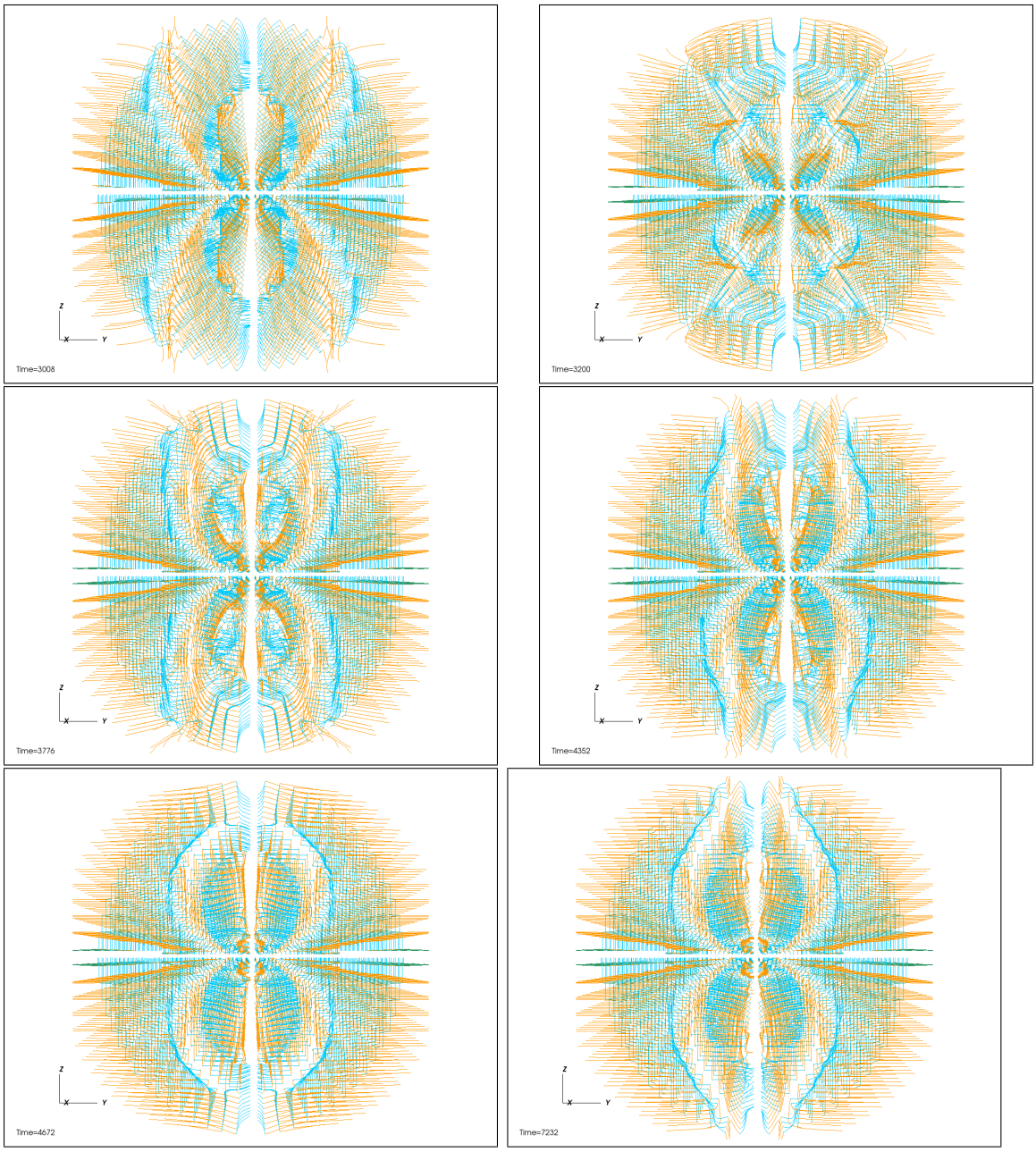

Figure 6: shows the vortex lines for a binary black hole merger with equal masses of 0.5 at different time frames: the blue, green, and orange lines indicate the three orthogonal vortex lines

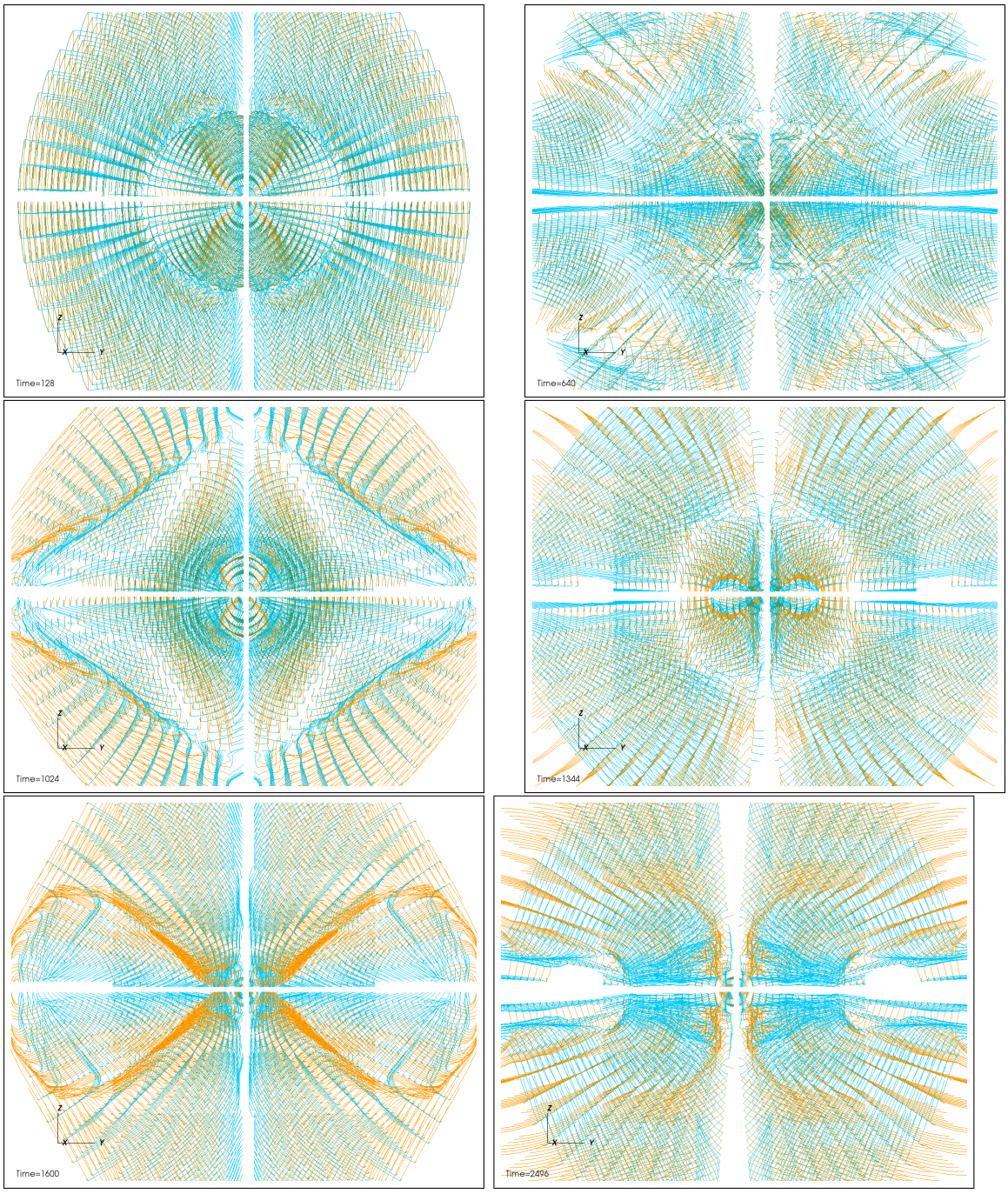
Time=128
Time=640
Time=1024
Time=1344
Time=1600
Time=2496

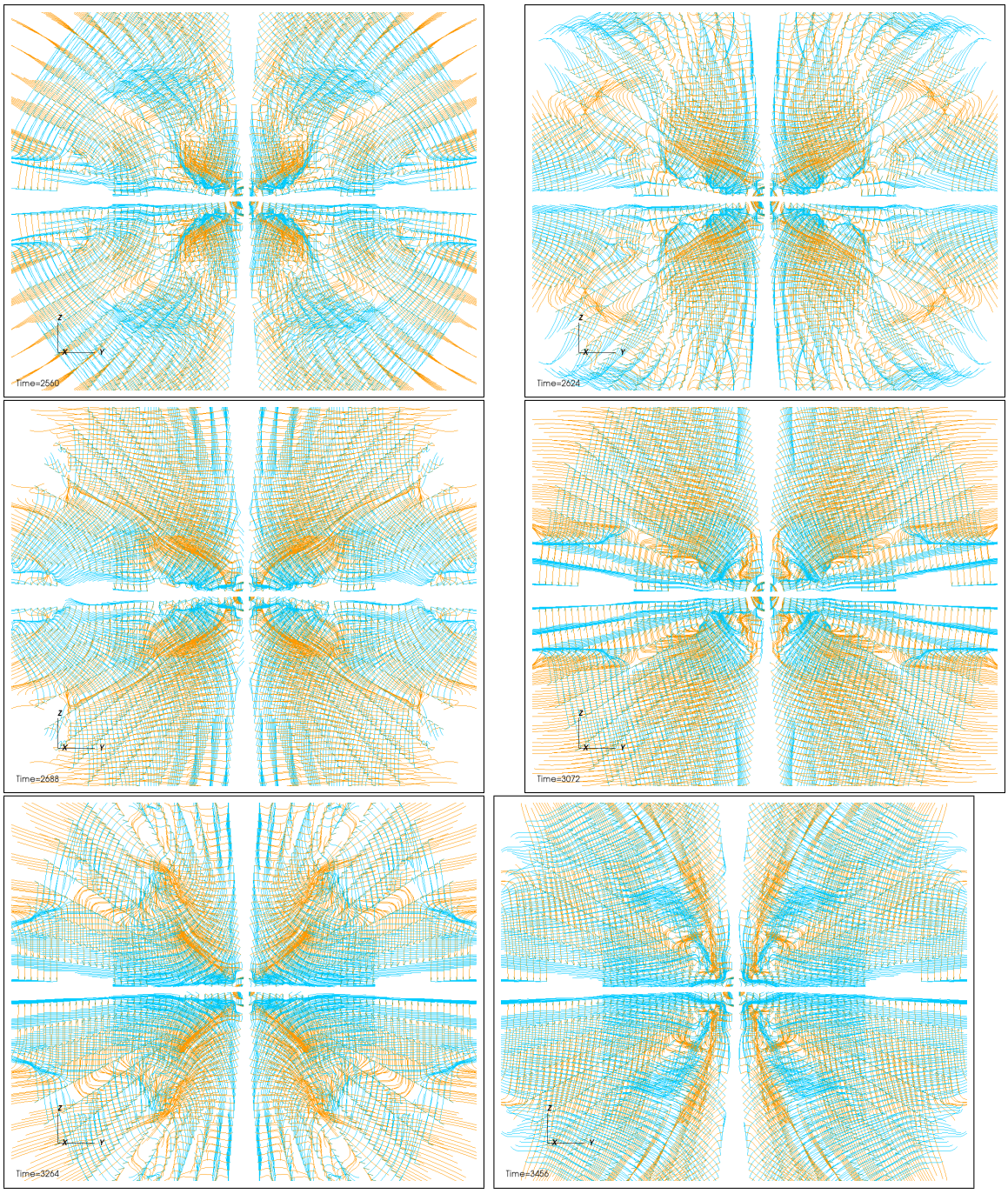
Time=2560
Time=2624
Time=2688
Time=3072
Time=3264
Time=3456

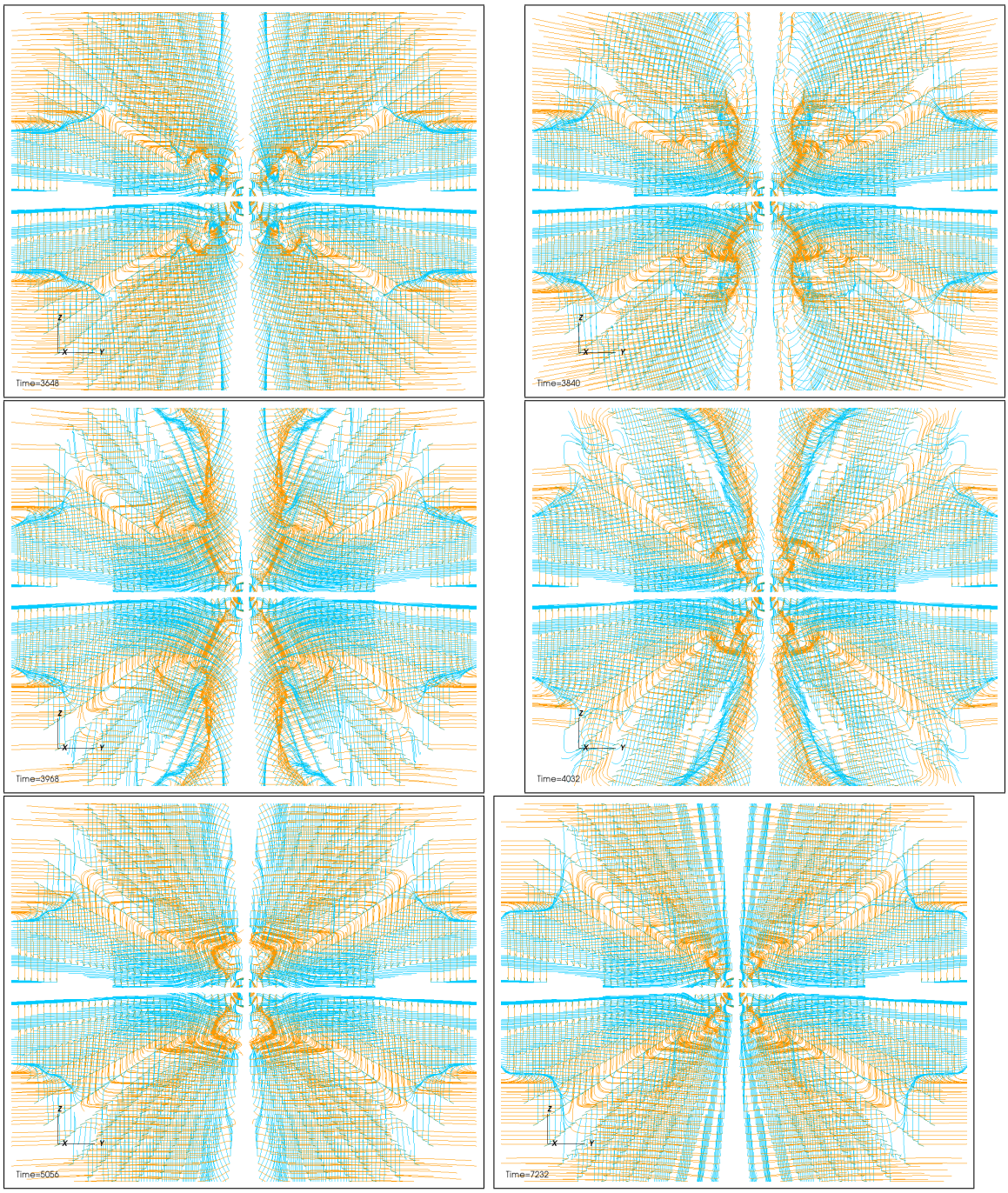

Figure 7: shows the tendex lines for a binary black hole merger with equal masses of 0.5 at different time frames: the blue, green, and orange lines indicate the three orthogonal tendex lines

5 Conclusion

In this paper, we spent a bit of time introducing the fundamentals of general relativity, tensor calculus, and differential geometry. We learned that the Riemann curvature tensor embodies all information about the curvature of spacetime, and from its contractions, we can formulate the Einstein field equations. The Einstein fields equations, as we have learned, relates the curvature of spacetime with the local stress, energy, and momentum. We have heard over and over again that these equations are very difficult to solve analytically, and we must use numerical relativity to solve them. We then discussed about the existence of gravitational waves and their most promising source – binary black hole collisions and mergers. We learned that in order to study gravitation waves, we must compare the receiving waves from the gravitational wave interferometers with vast waveform templates – which are generated through countless runs with different parameters. We then introduced the 3+1 slicings of the vacuum Riemann tensor, the Weyl tensor, into the electric and magnetic tensors $\mathcal{E}_{ij}$ and $\mathcal{B}_{ij}$. We called the electric tensor, the tidal field, which deals with the stretching and compressing of an observer, and the magnetic field, the frame-dragging field, which deals with the differential frame-dragging effects on an observer. We learned that when we take the integral curves of the eigenvectors of each tensor, we arrive at the tendex and vortex lines. And we learned that in regions of strong-gravity such the horizon of a black hole, the Weyl tensor, or just plainly curvature, can be fully characterized by these vortex and tendex lines. We derived the components of the $\mathcal{E}_{ij}$ and $\mathcal{B}_{ij}$ tensor analytically, and then used computers to solve the eigenfunctions and create the integral curves of these, numerically. We were able to visualize the spacetime curvature around a Schwarzschild black hole, a rotating Kerr black hole, and an equal-mass binary black hole merger using these tendex and vortex lines. From

these visuals we will be able to understand how gravitational waves can be generated through the dynamical evolutions of the system. Ultimately, this tool will be prove to be a useful tool for generating more accurate waveforms used for gravitational wave analysis.

References

[1] Kenneth A. Dennison and Thomas W. Baumgarte. Analytical tendex and vortex fields for perturbative black hole initial data, 2012.

[2] James Healy, Frank Herrmann, Ian Hinder, Deirdre M. Shoemaker, Pablo Laguna, and Richard A. Matzner. Superkicks in hyperbolic encounters of binary black holes. Phys.Rev.Lett.102:041101,2009, 2008.

[3] Wei-Tou Ni. Gravitational waves, dark energy and inflation. Mod.Phys.Lett.A25:922-935,2010, 2010.

[4] David A. Nichols, Aaron Zimmerman, Yanbei Chen, Geoffrey Lovelace, Keith D. Matthews, Robert Owen, Fan Zhang, and Kip S. Thorne. Visualizing spacetime curvature via frame-drag vortexes and tidal tendexes. iii. quasinormal pulsations of schwarzschild and kerr black holes. *Phys. Rev. D*, 86:104028, Nov 2012.

[5] Richard H. Price, John W. Belcher, and David A. Nichols. Comparison of electromagnetic and gravitational radiation; what we can learn about each from the other, 2012.

[6] Fan Zhang, Aaron Zimmerman, David A. Nichols, Yanbei Chen, Geoffrey Lovelace, Keith D. Matthews, Robert Owen, and Kip S. Thorne. Visualizing spacetime curvature via frame-drag vortexes and tidal tendexes. ii. stationary black holes. *Phys. Rev. D*, 86:084049, Oct 2012.

[7] J. B. Hartle. *Gravity : an introduction to Einstein's general relativity.* Addison-Wesley, San Francisco, 2003.

[8] Norbert Straumann. *General relativity.* Springer, Heidelberg New York, 2013.

[9] Albert Einstein. *Relativity : the special and the general theory; a popular exposition.* Martino Publishing, Mansfield Centre, CT, 2010.

[10] Hans Stephani. *General relativity : an introduction to the theory of the gravitational field.* Cambridge University Press, Cambridge England New York, 1990.

[11] Sean Carroll. *Spacetime and geometry : an introduction to general relativity.* Addison Wesley, San Francisco, 2004.

[12] Shlomo Sternberg. *Semi-Riemann Geometry and General Relativity.* University Press of Florida, Gainesville, Florida, 2009.

[13] John Walecka. *Introduction to general relativity.* World Scientific, Singapore Hackensack, NJ, 2007.

[14] Charles Misner. *Gravitation.* W.H. Freeman, San Francisco, 1973.

[15] Hooft. *Introduction to general relativity.* Rinton Press, Princeton, N.J, 2001.

[16] Bernard Schutz. *A first course in general relativity.* Cambridge University Press, Cambridge New York, 2009.

[17] Steven Weinberg. *Gravitation and cosmology : principles and applications of the general theory of relativity.* Wiley, New York, 1972.

[18] P. A. M. Dirac. *General theory of relativity.* Princeton University Press, Princeton, N.J, 1996.

[19] John Stewart. *Advanced general relativity.* Cambridge University Press, Cambridge England New York, 1993.

[20] L. P. Hughston. *An introduction to general relativity.* Cambridge University Press, Cambridge New York, 1990.

[21] David A. Nichols, Robert Owen, Fan Zhang, Aaron Zimmerman, Jeandrew Brink, Yanbei Chen, Jeffrey D. Kaplan, Geoffrey Lovelace, Keith D. Matthews, Mark A. Scheel, and Kip S. Thorne. Visualizing spacetime curvature via frame-drag vortexes and tidal tendexes: General theory and weak-gravity applications. *Phys. Rev. D*, 84:124014, Dec 2011.

[22] Thomas Baumgarte. *Numerical relativity : solving Einstein's equations on the computer*. Cambridge University Press, Cambridge New York, 2010.

[23] Bernard F Schutz and Franco Ricci. Gravitational waves, sources, and detectors. Schutz, B. F.; Ricci, F.: Gravitational Waves, Sources and Detectors. In: Gravitational Waves, Ciufolini, I, et al, eds. (Institute of Physics, Bristol, 2001), 2010.

[24] James Healy, Pablo Laguna, Larne Pekowsky, and Deirdre Shoemaker. Template mode hierarchies for binary black hole mergers, 2013.

[25] Larne Pekowsky, James Healy, Deirdre Shoemaker, and Pablo Laguna. Impact of higher-order modes on the detection of binary black hole coalescences, 2012.

[26] Robert Wald. *General relativity*. University of Chicago Press, Chicago, 1984.

[27] Robert Owen, Jeandrew Brink, Yanbei Chen, Jeffrey D. Kaplan, Geoffrey Lovelace, Keith D. Matthews, David A. Nichols, Mark A. Scheel, Fan Zhang, Aaron Zimmerman, and Kip S. Thorne. Frame-dragging vortexes and tidal tendexes attached to colliding black holes: Visualizing the curvature of spacetime. *Phys. Rev. Lett.*, 106:151101, Apr 2011.

[28] Aaron Zimmerman, David A. Nichols, and Fan Zhang. Classifying the iso-

lated zeros of asymptotic gravitational radiation by tendex and vortex lines. Phys.Rev.D84:044037,2011, 2011.

[29] Kenneth A. Dennison and Thomas W. Baumgarte. Invariants for tendex and vortex fields, 2012.

[30] Frank Löffler, Joshua Faber, Eloisa Bentivegna, Tanja Bode, Peter Diener, Roland Haas, Ian Hinder, Bruno C. Mundim, Christian D. Ott, Erik Schnetter, Gabrielle Allen, Manuela Campanelli, and Pablo Laguna. The einstein toolkit: A community computational infrastructure for relativistic astrophysics, 2011.